PCCP

Metalloradical complex Co-C•Ph3 catalyzes the CO2 reduction in gas phase: a theoretical study

Journal:	*Physical Chemistry Chemical Physics*
Manuscript ID	CP-ART-08-2020-004453.R2
Article Type:	Paper
Date Submitted by the Author:	29-Nov-2020
Complete List of Authors:	Tang, Chuangkai; Huaibei normal university Li, Yazhou; Huaibei normal university Zhou, Zhong-Jun; Institute of Theoretical Chemistry, Jilin University, Ma, Fang; Huaibei normal university, Mo, Yirong; University of North Carolina at Greensboro, Department of Nanoscience, Joint School of Nanoscience and Nanoengineering

Metalloradical Complex Co-C•Ph_3 Catalyzes the CO_2 Reduction in Gas Phase: A Theoretical Study

Chuan-Kai Tang,[a] Ya-Zhou Li,[a] Zhong-Jun Zhou,[b] Fang Ma*[a] and Yirong Mo*[c]

[a] School of Chemistry and Materials Science, Huaibei Normal University, Huaibei, 235000, China. *E-mail: mafangchem@foxmail.com*

[b] Institute of Theoretical Chemistry, Jilin University, Changchun, 130023, China.

[c] Department of Nanoscience, Joint School of Nanoscience and Nanoengineering, University of North Carolina at Greensboro, Greensboro, NC 27401, USA. *E-mail: y_mo3@uncg.edu*

Abstract

Metal-stabilized radicals have been increasingly exploited in modern organic synthesis. Here, we theoretically designed a metalloradical complex Co-C$^{\bullet}$Ph$_3$ with the triplet characters through the transition metal cobalt (Co^0) coordinating a triphenylmethyl radical. The potential catalytic role of this novel metalloradical in the CO_2 reduction with H_2/CH_4 in gas phase was explored by performing density functional theory (DFT) calculations. For the CO_2 reduction reaction with H_2, there are two possible pathways. One (path A) is the activation of CO_2 by Co-C$^{\bullet}$Ph$_3$, followed by the hydrogenation of CO_2. The other (path B) starts from the splitting of the H-H bond by Co-C$^{\bullet}$Ph$_3$, leading to the transition-metal hydride complex CoH-H which can reduce CO_2. DFT computations show that path B is more favorable than path A as their rate-determining free energy barriers are 18.3 and 27.2 kcal/mol, respectively. For the reduction of CO_2 by CH_4, however, two different products, CH_3COOH and $HCOOCH_3$, can be generated following different reaction routes. Both routes begin with one CH_4 molecule approaching the metalloradical Co-C$^{\bullet}$Ph$_3$ to form the intermediate CoH-CH_3. This intermediate can evolve following two different pathways, depending on whether the H bonded to Co is transferred to the O (pathway **PO**) or the C (pathway **PC**) of CO_2. Comparing their rate-determining steps, we identified that the **PO** route is more favorable for the reduction of CO_2 by CH_4 to CH_3COOH with the reaction barrier 24.5 kcal/mol. Thus, the present Co^0-based metalloradical system represents a viable catalytic protocol that can contribute to the effective utilization of small molecules (H_2 and CH_4) to reduce CO_2, and provides an alternative strategy in the exploration of the CO_2 conversion.

1. Introduction

There have been growing interests in the development of metalloradical catalysts (MRCs),[1-4] which can provide catalytic initiation and selective control in many chemical syntheses and contribute to the discovery of new catalytic pathways for stereoselective reactions. MRC is a kind of metalloradical complexes as open-shell catalysts for generating metal-supported organic radicals and controlling. Early in 2005, Grützmacher[5] showed that transition metal (Rh(I)) coordination supports an aminyl radical, where electron paramagnetic resonance spectroscopy and density functional theory confirm the 57% localization of the unpaired spin at N. Since then, plentiful stable metalloradical catalysts have been reported, for example, Ti(III)-based MRC[6, 7]， Co(II)-based MRC[8-10]， and so on. Notably, the Zhang group has developed a family of unique Co(II)-based metalloradical catalysts with tunable electronic, steric, and chiral environments. These Co(II)-based MRCs have shown to be highly effective for a wide range of stereoselective organic reactions, including the catalytic asymmetric radical cyclopropanation of alkenes[11, 12] and catalytic radical C–H amination[13, 14]. Bas de Bruin et al. proposed the mechanism for catalytic ketene synthesis via Co(III)-carbene radical carbonylation,[4] whereas Gansäuer et al. exploited the innate ability of titanocene(III)-based catalysts to realize both oxidative addition and reductive elimination in single electron steps[6, 7]. Similarly, many other groups[15, 16] have also contributed to the synthesis of metalloradical complexes and their broad applications in catalysis.

One of the current research frontiers is the CO_2 reduction, which is of imperative and enormous interests and implications. The chemical transformation of CO_2 into value-added chemicals has been considered important for creating a sustainable low-carbon economy. However, there are challenges to achieve this ideal goal of a green low-carbon cycle, largely due to the inertia of CO_2. To reduce CO_2 to useful chemical products, transition-metal-catalyzed CO_2 transformations have been regarded as a powerful and realistic tool.[17-21] Among various routes of CO_2 reduction, the CO_2 hydrogenation/insertion reaction with 100% atom economy is a particularly significant route for CO_2 utilization. Most hydrogenations of CO_2 to formic acid rely

on effective catalysts involving precious metals such as ruthenium,[22-24] rhodium[25, 26], and iridium[27, 28]. Alternatively, frustrated Lewis pairs (FLPs)[29], N-heterocyclic carbenes[30, 31] and ethynyl dithiocarbamate species[32] have been synthesized and applied to CO_2 hydrogenation/insertion reactions. The direct C-C coupling of CO_2 with CH_4 to form acetic acid is another attractive route. A general stepwise method has been proposed to convert CO_2 and CH_4 into acetic acid over Cu/Co-based catalysts,[33] Pd/C, Pt/Al_2O_3,[34] Pd/SiO_2, and Rh/SiO_2[35] by heterogeneous catalysis. Recently, Zhao et al. investigated the direct C-C coupling through CO_2 inserting into the σ_{C-H} bond of CH_4 by using Zn-doped ceria catalyst.[36]

In this work, we intended to develop a different strategy for the CO_2 hydrogenation/insertion reaction through the concept of metalloradicals (see **c** in Scheme 1) and validate the potentials of the designed metalloradical by performing DFT computations. Although increasing reports on metalloradical catalysts have already stimulated increasing endeavors in this field, there are still many uncharted research fields to be explored. For instance, to our knowledge, there has been no report on any metalloradical complex involving a neutral transition metal (M(0)) coordination to a radical so far. As such, we proposed a new metalloradical Co-C$^{\bullet}Ph_3$ based on the neutral transition metal cobalt and the triphenylmethyl radical. The latter is the first relatively stable free radical ever reported.[37] Even more interesting is the exploration of this new theoretically designed metalloradical's potential applications in the CO_2 reduction. There are two outstanding advantages of the proposed metalloradical. One is that it may serve not only as an initiator of CO_2 reduction, but also as a supporter of $CO_2^{\bullet-}$ moiety in the reactant or intermediate. The other is that the metalloradical is able to provide transition metal hydrogen complexes (TMHCs), which can serve as important intermediates in the catalytic transfer of protons, hydrogen atoms,[38, 39] hydrides,[40, 41] or electrons[42, 43] to substrates from H_2. Therefore, novel metalloradicals may be a fascinating tool for providing the hydride source in CO_2 hydrogenation, and metalloradical catalytic systems are expected to enhance the efficiency and economic feasibility of CO_2 transformations. Scheme 2 illustrated the two possible routes (Path A with CO_2 binding to the catalyst first and Path B with H_2/CH_4 binding to the catalyst first)

of CO_2 reduction catalyzed by Co-C•Ph_3. This metalloradical catalytic process is applicable for the CO_2 reduction with small molecule (H_2 and CH_4), offering a direct method for CO_2 inserting into the H-R bond (R=H and CH_3). We note, however, that the formation of the metalloradical Co-C•Ph_3 has not realized experimentally, and this theoretical study provides a perspective for an alternative strategy for the CO_2 reduction and an extension of the potential catalytic applications of metalloradical complexes.

Scheme 1. Strategies for CO_2 activation by using a radical or metalloradical.

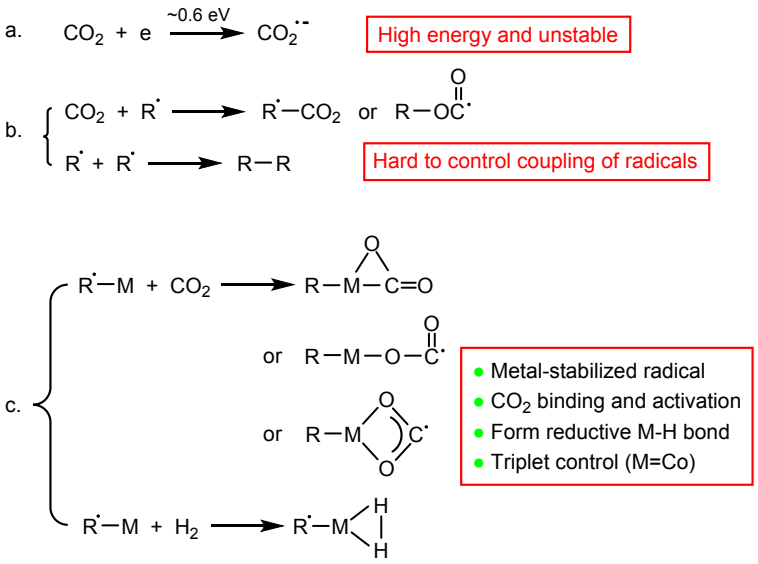

Scheme 2. Two paths of CO_2 reduction catalyzed by the metalloradical Co-C•Ph_3 with a triplet ground state.

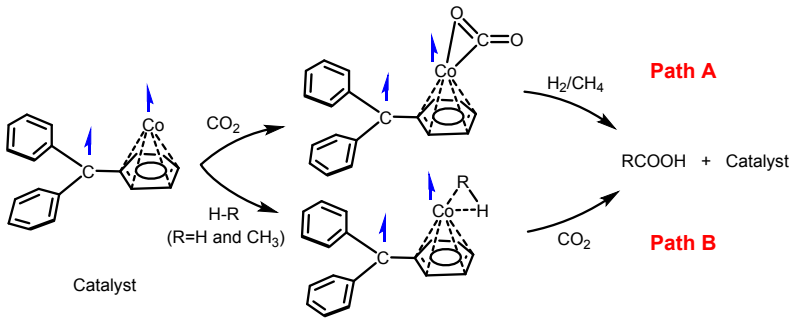

2. **Computational details**

All the calculations were performed with the GAUSSIAN 16 programs.[44] The geometrical optimizations of the reactants, intermediates, transition states (TSs) and products were performed with the density functional exchange correlation (B3LYP) method[45,46] including the empirical dispersion corrections developed by Grimme et al.[47, 48], and the combination of the Def2TZVP basis set for Co atom and the augmented correlation consistent basis set 6-311+G(d) for all nonmetal atoms.[49] Vibrational frequency calculations at the same level were performed to confirm stationary points as minima (zero imaginary frequency) or transition states (one imaginary frequency). In several cases where the TSs could not be easily confirmed by the animation of their vibrations, intrinsic reaction coordinate (IRC)[50, 51] calculations were performed to establish the connection of each TS to its corresponding reactant and product. In addition, partial atomic charges were calculated with the natural population analysis (NPA)[52-54] at the same level of the geometrical optimizations.

3. Results and discussion

3.1 Metalloradical Co^0-$C^{\bullet}Ph_3$ at the triplet ground state

The partially vacant d orbitals make transition metals tend to play a dual role in bonding ligands as both electron donor and acceptor, leading to the delocalization effect and regioselectivity protection and providing means for supporting the stability of a radical such as triphenylmethyl. Fig. 1 depicts the optimized structures of the metalloradical Co-$C^{\bullet}Ph_3$ at the singlet and triplet states. The formation of the triplet structure is an exergonic process with the decreasing of Gibbs free energy by 17.6 kcal/mol, while the formation of the singlet structure is an endergonic process with the increasing of Gibbs free energy by 12.9 kcal/mol. Thus, the transition metal cobalt is able to considerably stabilize the radical $C^{\bullet}Ph_3$ in the formation of the triplet state. The singlet-triplet free energy gap for Co-$C^{\bullet}Ph_3$ is 31.5 kcal/mol, favoring the triplet state considerably. This seems conflict with our commonsense. According to chemical bond theory, two parts with unpaired electrons tend to form a covalent bond by sharing two electrons

and eventually favor the singlet state. In the present case, both Co and C•Ph$_3$ have odd (unpaired) electrons and thus it is inclined to form a close-shell singlet state with a C-Co bond. However, computations show that Co-C•Ph$_3$ has an open-shell triplet ground state. Thus, it is intriguing to figure out what is the governing force for the stability of the triplet state of Co-C•Ph$_3$. In general, the preference of a triplet state over its singlet counterpart comes from two nearly degenerate orbitals for two electrons.

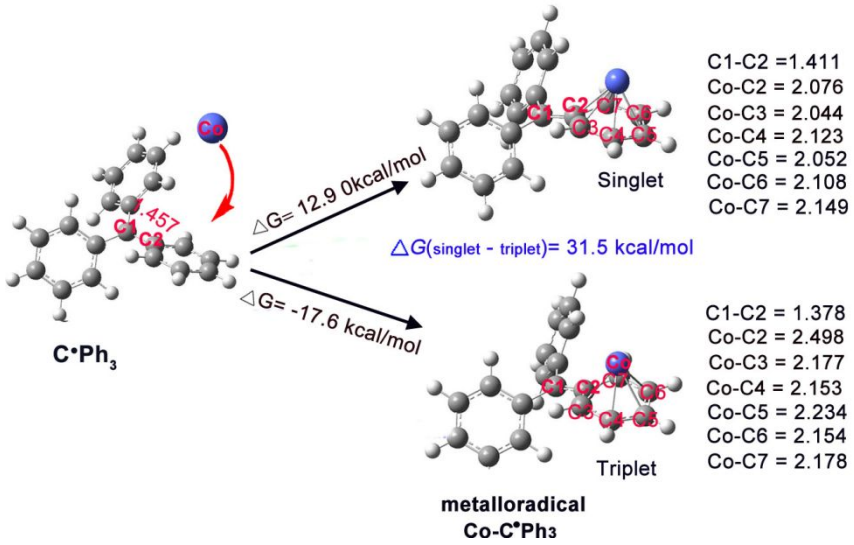

Fig. 1 The formation of metalloradical **Co-C•Ph$_3$** with the triplet characters. The bond distances are given in Å.

The optimized structure of Co-C•Ph$_3$ at the triplet state shows that the Co atom is located above one benzene ring in the form of η^6, and not directly bonded with the radical center C1 of Co-C•Ph$_3$. However, the C1-C2 bond length (1.378 Å) in the complex Co-C•Ph$_3$ is noticeably shorter than the distance (1.457 Å) in C•Ph$_3$, suggesting considerable electron (spin density) delocalization from C1 to the benzene ring bonded to Co. Indeed, as shown in Fig. 2, both SOMOs of Co-C•Ph$_3$ (including α and β orbitals, see Fig S1 in ESI) are close in energy with a gap of only 6.9 kcal/mol and contributed from d_z-π interactions and π orbitals C•Ph$_3$. Of particularly, the C1-C2 bond exhibits certain double bond characters, due to the π-π orbital interactions. NBO computations also revealed that secondary orbital interactions between the

antibond orbital of the C1-C2 bond and the bond orbitals of C3-Co and C4-Co stabilize the complex (through the C1-C2 bond) by 15.2 kcal/mol. The d_z-π interaction in Co-C•Ph_3 guides Co interacting with C•Ph_3, and the NPA showed that there is significant electron transfer from Co to the concerned benzene ring by ~0.6 e.

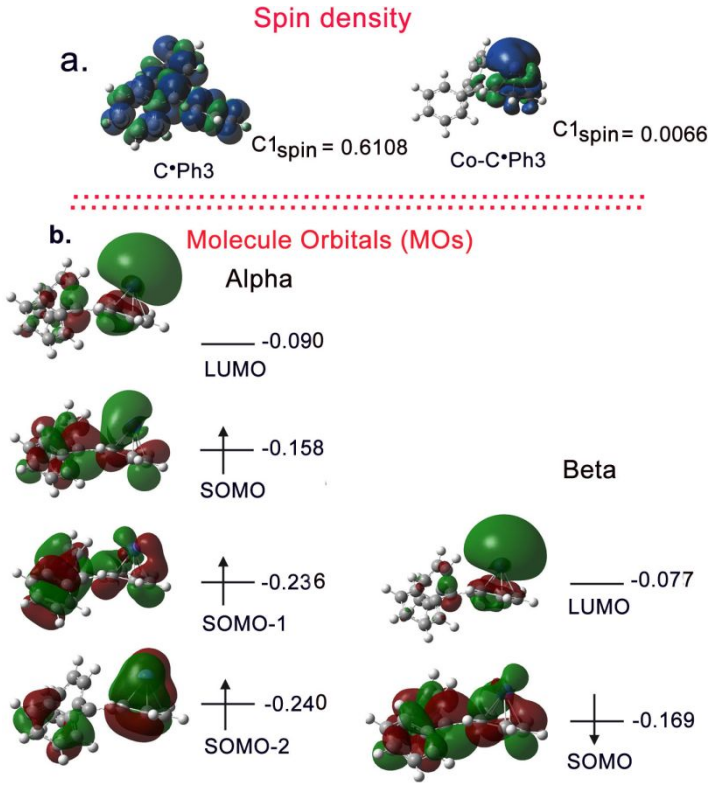

Fig. 2 (**a**) Spin density maps of the radical C•Ph_3 and metalloradical Co^0-C•Ph_3, including the spin density values on C1 atom; (**b**) frontier orbitals of Co^0-C•Ph_3, including α orbitals and their corresponding β orbitals.

In consistent with the relative stability of the triphenylmethyl radical, computations showed that the majority of the spin density in C•Ph_3 is delocalized over the whole molecular skeleton. This high delocalization prohibits the combination of two C•Ph_3 units to Ph_3C-CPh_3. For Co-C•Ph_3, as shown in Fig. 2a, the majority of the spin density is resided on the Co atom and its bonding benzene rings, with a minority of spin density on the C1 atom. Thus, the spin density (0.0066) on the C1 atom in Co-C•Ph_3 decreases in comparison with that in C•Ph_3 (0.6108),

which makes the dimerization of two metalloradicals even more difficult. In other words, Co-C•Ph_3 is expected to be more stable than C•Ph_3. As a stable metalloradical at the triplet ground state, Co-C•Ph_3 possesses both advantages of transition metal catalysts and radical characters. In brief, the metalloradical Co-C•Ph_3 has the potential of being a promising catalyst for reducing CO_2.

It should be pointed out that utilizing surrounding ligands completing the coordination sphere of the concerned transition metal might provide further stability of a metalloradical complex. For the present work, we employed either bipyridyl or pentane-2,4-diimine as the σ-donor ligand to stabilize the metalloradical Co-C•Ph_3. The optimized structures with geometric parameters are provided in Electronic Supplementary Information (ESI) as Figs. S2 and S3. Notably, the triplet structure maintains a lower energy than the singlet structure in both cases. We also attempted to investigate their catalytic role in the CO_2 reduction. But the complexes of Co-C•Ph_3 with both ligands fail to activate CO_2 or H_2 molecules (see Figs. S4 and S5 in ESI). This indicates that these σ-donor ligands may increase the electron deficiency of the transition metal, therefore weakening the reactivity of Co-C•Ph_3. However, the steric effect may also play a role. To identify the role of either electronic or steric effects therein, we further performed computations with π-acceptor ligands (CO or ethylene) coordinating to the metalloradical Co-C•Ph_3 (see Figs. S6 and S7 in ESI). Similar to the σ-donor ligands, the π-acceptor ligands also weaken the reactivity of Co-C•Ph_3. Accordingly, we believe that the steric hindrance effect is the primary cause for weakening the reactivity of Co-C•Ph_3. Notably, the structure of Co-C•Ph_3 varies little with the coordination of any ligands, suggesting that the d-π interaction between the Co atom and one benzene ring is intact, as the Co atom is located above one benzene ring in the form of η^6 in the metalloradical Co-C•Ph_3.

3.2 Hydrogenation of CO_2 catalyzed by metalloradical Co^0-C•Ph_3

Considering that the metalloradical Co-C•Ph_3 possesses both advantages of transition metal catalysts and radical characters, here we computationally explored its catalysis in the

hydrogenation of CO_2. As described in Scheme 2, there are two possible routes for the CO_2 hydrogenation, based on the sequence of adding H_2 and CO_2 to the catalyst. For the first route (denoted as path A), CO_2 is added first. The whole process is initiated with one CO_2 molecule coordinated to the transition-metal center Co atom of the metalloradical Co^0-$C^{\bullet}Ph_3$ through d-π interaction to form a Co-CO_2 complex and Fig. 3 shows the optimized structure. This binding step is exergonic with the standard Gibbs free energy change ($\triangle G^0$) of -9.6 kcal/mol. For the second route (denoted as path B), H_2 is similarly coordinated to the transition metal Co, forming CoH-H (shown in Fig. 3) where there are two cobalt hydride bonds (Co-H) via the transition state $TS_{CoH\text{-}H}$ (see Fig. S8 in ESI). This step is also exergonic by -7.6 kcal/mol. It should be noted that both CoH-H and Co-CO_2 complexes are triplet, as their corresponding singlet states are disfavored by 19.7 and 10.1 kcal/mol, respectively. By binding to Co^0-$C^{\bullet}Ph_3$, CO_2 is significantly activated as in the intermediate Co-CO_2 it exhibits a bent structure with the OCO angle 142º and elongated C-O bonds by 0.03~0.1 Å from a free linear CO_2. In the structure of CoH-H, the H-H bond is splitted to 2.371 Å from 0.740 Å in the isolated H_2 molecule. These structural characteristics suggest that both CO_2 and H_2 are activated by binding to the metalloradical Co^0-$C^{\bullet}Ph_3$.

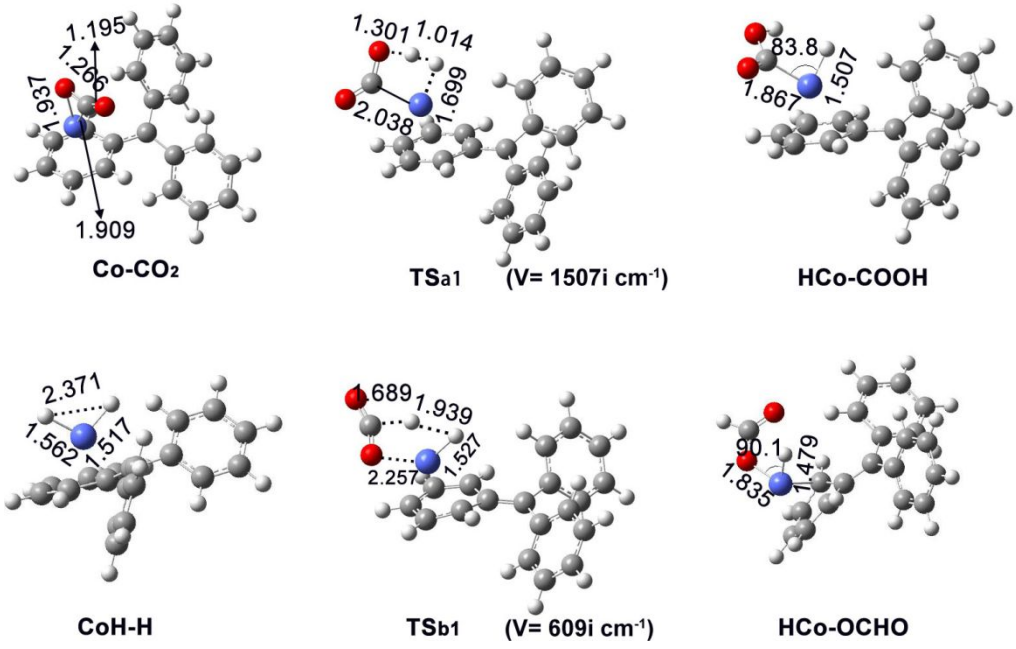

Fig. 3 Optimized geometries of the intermediates and key transition states in the process of CO_2 hydrogenation. The bond distances are given in Å.

According to Scheme 2, the next step is the addition of the second reactant. For path A, the complex Co-CO_2 would react with H_2 to form a key intermediate HCo-COOH through the transition state TS_{a1}. For path B, CO_2 approaches CoH-H to form a key intermediate HCo-OCHO through the transition state TS_{b1}. Computations showed that the formation of HCo-OCHO is both kinetically and thermodynamically favored over the formation of HCo-COOH, as the addition of CO_2 to CoH-H requires to overcome an energy barrier of 18.3 kcal/mol whereas the addition of H_2 to Co-CO_2 needs 27.2 kcal/mol. Further, the intermediate state HCo-OCHO is more stable than HCo-COOH by 8.8 kcal/mol. These results highlight the significance of sequence in adding H_2 and CO_2 to the catalyst Co^0-C$^\bullet$$Ph_3$. Fig. 3 shows the optimized geometries of key structures. In TS_{a1} for path A, the H-H bond is essentially splitted by both O and Co atoms of Co-CO_2 as the H-H distance is 1.014 Å. The splitted hydrogen atoms are bonded to the O and Co atoms, respectively, and the O-H distance is 1.301 Å and the H-Co distance is 1.699 Å. The transition state TS_{b1} for path B is different from TS_{a1} in that CO_2 molecule is coordinated by the H and Co atoms of CoH-H. The C-H distance is 1.689 Å, and the O-Co distance is 2.257 Å. Between the intermediates HCo-OCHO and HCo-COOH, the notable difference lies in the formed moieties -OCHO and -COOH, respectively. In HCo-COOH, the C-Co and H-Co distances are 1.867 Å and 1.507 Å, respectively, and their intersection angle is only 83.8º. But in HCo-OCHO, the O-Co and H-Co distances are 1.835 Å and 1.479Å, respectively, and their intersection angle is 90.1º.

To complete the CO_2 hydrogenation, it is necessary to have the hydride ion transferred from the Co site to the moiety -HCOO or -COOH from the intermediate HCo-OCHO or HCo-COOH, respectively. In both cases, the hydride ion transfer goes through transition states (labelled as TS_{a2} and TS_{b2}) which are characterized with a three-membered ring mode, as depicted in Fig. 4. However, we found that the energy barrier of TS_{b2} is higher by ~8 kcal/mol

than that of TS_{a2}. Two factors may contribute to the higher barrier for path B than for path A in this step. First, the hydride ion transfer occurs from the Co site to the positively charged C of the moiety -COOH in TS_{a2}. But in TS_{b2}, the transfer is from the Co site to the negatively charged O of the moiety -HCOO. Second, the intermediate HCo-OCHO has a lower energy by 8.8 kcal/mol than HCo-COOH. Therefore, we found that the hydride ion transfer from the Co site to the moiety -COOH is more favorable than to the moiety –HCOO. With the hydride ion transferred, the same final product, HCOOH, is produced. Fig. 5 plots the energy flow charts for both reaction pathways.

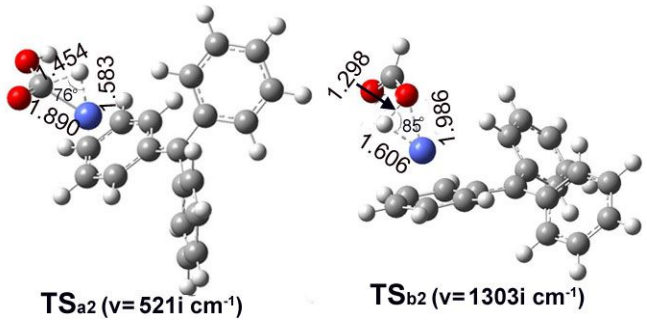

Fig. 4 Optimized hydride ion-transfer transition states $\mathbf{TS_{a2}}$ and $\mathbf{TS_{b2}}$. The bond distances are given in Å.

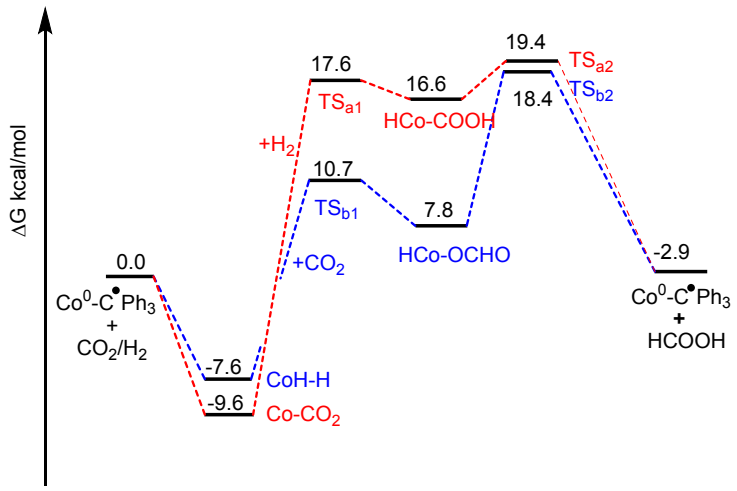

Fig. 5 Pathways (path A in red and path B in blue) for the CO_2 hydrogenation catalyzed by metaloradical Co^0-C•Ph_3.

Fig. 5 shows that for path A, the rate-determining step is the formation of the key intermediate HCo-COOH with the energy barrier of 27.2 kcal/mol. Similarly, for path B, the rate-determining step is the formation of the key intermediate HCo-OCHO with the total barrier of 18.3 kcal/mol. By comparing these two reaction pathways, we found that the path B is more favorable for the CO_2 hydrogenation than the path A.

Herein, it would be interesting to examine the CO_2 hydrogenation catalyzed by the complex $Co(C_6H_6)$ (or B-Co in short) which is formed through the transition metal (Co^0) coordinating a benzene molecule. The formation of the B-Co complex is a slightly exergonic process with the decreasing free energy of 4.3 kcal/mol. Similar to the CO_2 hydrogenation catalyzed by metalloradical Co^0-C$^\bullet$$Ph_3$, there are two possible reaction routes based on the sequence of adding H_2 and CO_2. One (path A) is that CO_2 molecule is first coordinated to the transition-metal center Co to form the complex B-Co-CO_2, while the other (path B) is that one H_2 molecule is first adsorbed by Co to form the complex B-Co-H_2. The further addition of H_2 to B-Co-CO_2 and CO_2 to B-Co-H_2 complete the CO_2 hydrogenation. Computations identified that the first step the addition (either CO_2 or H_2) is the rate-determining step in both reaction pathways (see Fig. 6). The CO_2 addition requires an energy barrier of 42.1 kcal/mol whereas the H_2 coordination goes over an energy barrier of 55.4 kcal/mol. Both the energy profile and optimized key transition states are depicted in Fig.7. We note that both reaction barriers in the CO_2 hydrogenation catalyzed by B-Co are much higher than the corresponding values in the hydrogenation process of CO_2 catalyzed by metalloradical (Co-C$^\bullet$$Ph_3$), respectively. This suggests that the metalloradical Co-C$^\bullet$$Ph_3$ may be a more appropriate candidate as a catalyst for reducing CO_2.

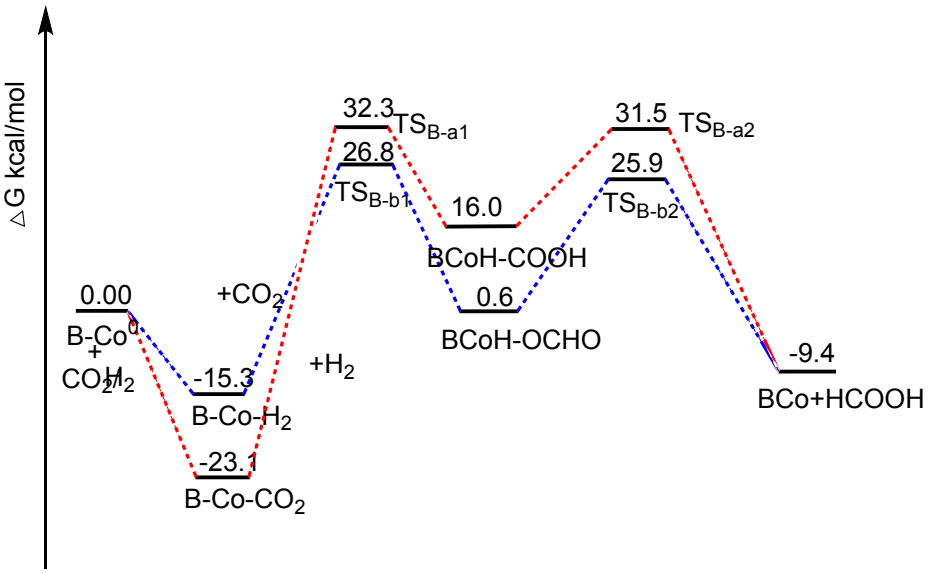

Fig. 6 The pathways of CO_2 hydrogenation catalyzed by the complex B-Co.

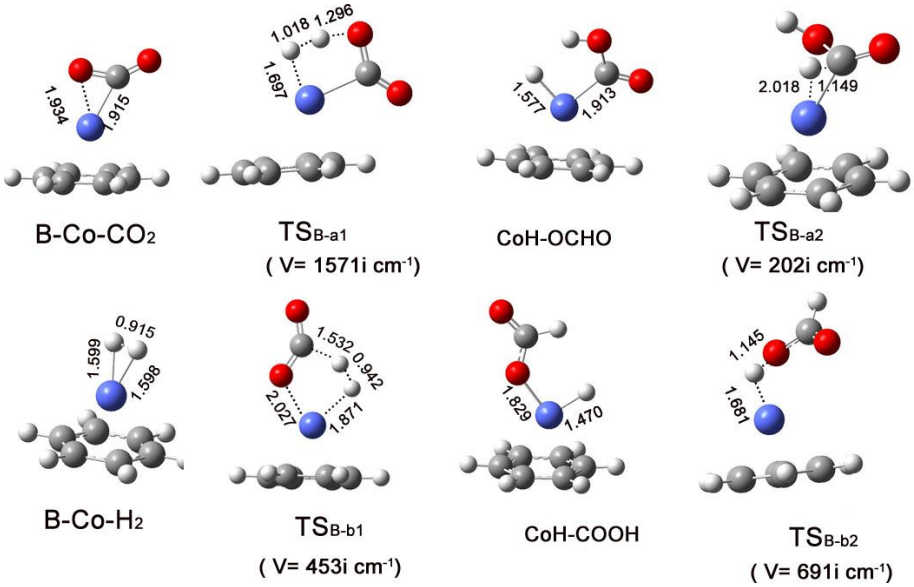

Fig. 7 Optimized intermediates and key transition states in the process of CO_2 hydrogenation catalyzed by the complex B-Co.

3.3 Conversion of CO_2 and CH_4 catalyzed by metalloradical Co^0-C•Ph_3

Here we continued to study the reduction of CO_2 by CH_4 catalyzed by the metaloradical Co^0-C•Ph_3 with the triplet characters. The combination of CO_2 and CH_4 may result in acetic acid and methyl formate. The reaction initiates from the approaching of one CH_4 molecule to the

metaloradical Co^0-$C^{\bullet}Ph_3$ by forming a slightly less stable intermediate CoH-CH_3, through a quick hydrogen transfer from CH_4 to the Co atom via the transition state TS_{CH3-H}. The reaction barrier for this initial step is only 10.1 kcal/mol, suggesting the efficient breaking of the C-H bond of CH_4 by Co^0-$C^{\bullet}Ph_3$. This is comparable to the metalloradical activation of methane studied by Sherry and Wayland,[55] whose approach extended the range of C-H bond reactions for rhodium(II) porphyrin complexes. The optimized structures of the intermediate CoH-CH_3 and the transition state TS_{CH3-H} are shown in Fig 8. At this point, a legitimate question is why the conversion of CO_2 and CH_4 to acetic acid does not begin with the absorption of CO_2 by the metalloradical Co^0-$C^{\bullet}Ph_3$. In the pretext, we showed that CO_2 molecule can interact with Co^0-$C^{\bullet}Ph_3$ through the d-π interaction to form Co-CO_2 with the decreasing of the free energy by 9.6 kcal/mol. For the subsequent reaction with H_2, there is a free energy barrier 27.2 kcal/mol. In the present case where the subsequent reaction is with CH_4, our computations showed that the free energy barrier is more than 40 kcal/mol, leading to the reaction essentially prohibited under mild conditions. Hence, in the following, we focused on the preferential intermediate CoH-CH_3, which represents a kind of transition metal hydrogen complexes (TMHCs), to reduce CO_2.

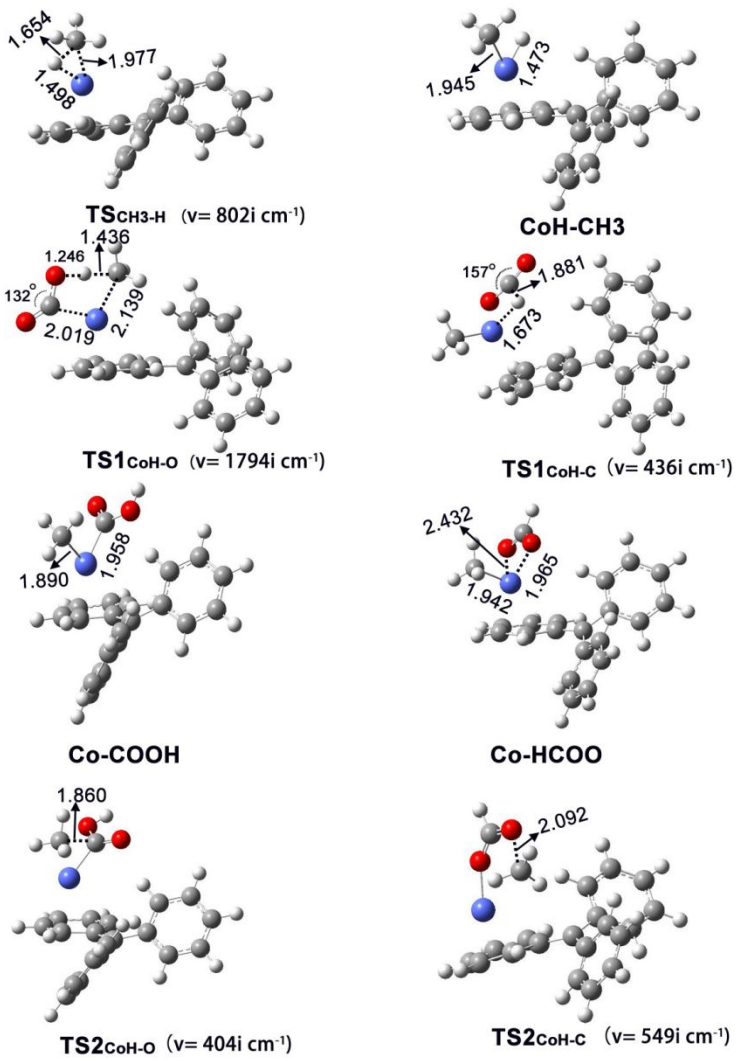

Fig. 8 Optimized intermediates and key transition states in the conversion of CO_2 and CH_4. The bond distances are given in Å

With the formation of CoH-CH_3, the Co-H bond therein can be employed to reduce CO_2 through hydrogen transfer from the Co site to CO_2. There are two likely reaction routes in this step, involving different transition states $TS1_{CoH-O}$ and $TS1_{CoH-C}$ whose optimized structures are shown in Fig.9. These two transition states generate different intermediates, including Co-COOH and Co-HCOO. $TS1_{CoH-O}$ concerns a hydrogen transfer from Co to the O of CO_2 (denoted as pathway **PO**) and $TS1_{CoH-C}$ corresponds to a hydrogen transfer from Co to the C of CO_2 (denoted as pathway **PC**). These two routes are dramatically different, with energy barriers of 24.5 and 6.5

kcal/mol, respectively. The generated intermediate Co-HCOO via the lower barrier is more stable by 12.7 kcal/mol than Co-COOH via the higher barrier. Therefore, the **PC** route is more favorable than the **PO** route.

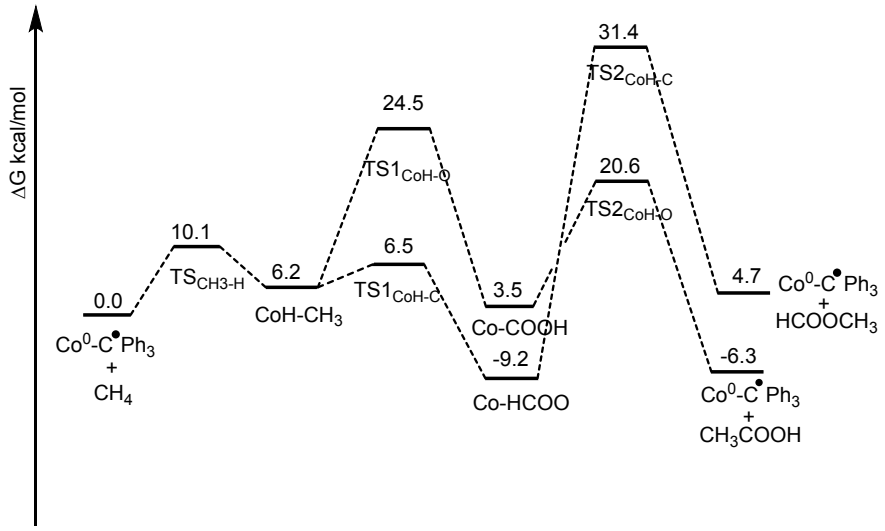

Fig. 9 Pathways for the conversion of CO_2 and CH_4 catalyzed by metalloradical Co^0-$C^{\bullet}Ph_3$.

To accomplish the conversion of CO_2 and CH_4, it is necessary to transfer the CH_3 radical from the Co site to the moiety -HCOO and -COOH, respectively. The CH_3 radical transfer experiences two transition states $TS2_{CoH-C}$ and $TS2_{CoH-O}$ (shown in Fig. 8) from two different intermediates Co-HCOO and Co-COOH, respectively. $TS2_{CoH-O}$ refers to the CH_3 radical transfer from the Co site to the positively charged C of the moiety –COOH, and $TS2_{CoH-C}$ corresponds to the CH_3 radical transfer from the Co site to the negative O of the moiety -HCOO. Since the intermediate Co-HCOO is more stable by 12.7 kcal/mol than Co-COOH but $TS2_{CoH-C}$ is of higher energy than $TS2_{CoH-O}$, we found that the CH_3 radical transfer from the Co site to the C of–COOH resulting in CH_3COOH is far more efficient than the transfer from the Co site to the O of –HCOO leading to $HCOOCH_3$. Fig. 9 plots the whole energy profiles for two reaction routes.

In summary, we computationally studied the conversion of CO_2 and CH_4 catalyzed by the metalloradical Co^0-$C^{\bullet}Ph_3$. Two different products, CH_3COOH and $HCOOCH_3$, are possible following two different reaction routes (**PO** versus **PC**). Both routes begin with one CH_4

molecule approaching to the metalloradical Co^0-C•Ph_3 and forming a slightly less stable intermediate CoH-CH_3, but the subsequent pathways are different, depending on whether the H atom bonded to the Co center is transferred to the O (**PO**) or the C of CO_2 (**PC**). The hydrogen transfer from the Co site to the C of CO_2 ($TS1_{CoH-C}$) is more favorable than from the Co site to the O of CO_2 ($TS1_{CoH-O}$). But in the following step of the CH_3 radical transfer, $TS2_{CoH-C}$ is of higher energy than $TS2_{CoH-O}$. Putting all steps together and examining the rate-determining steps, we found that the reaction route concerning the hydrogen transfer from the Co site to the O of CO_2 is more favorable than the alternative route involving the hydrogen transfer from the Co site to the C of CO_2 both thermodynamically and kinetically. In fact, the reaction of CO_2 and CH_4 catalyzed by Co^0-C•Ph_3 can only result in acetic acid.

Conclusion

In this prospect work, we proposed an innovative strategy to study the conversion of CO_2 with H_2/CH_4 catalyzed by the theoretically designed metalloradical complex (Co-C•Ph_3). This metalloradical is formed through the neutral transition metal (Co^0) coordinating to a triphenylmethyl, and is stable and of the triplet characters. Due to the unique properties, Co-C•Ph_3 is expected to be applicable in the CO_2 reduction. DFT computations showed that there are two possible reaction pathways for the reduction of CO_2 with H_2. The first pathway (path A) starts from the activation of CO_2 by Co-C•Ph_3, leading to an intermediate state Co-CO_2 which further reacts with H_2 to complete the hydrogenation cycle. The second pathway (path B) begins with the bond breaking of the hydrogen molecule by Co-C•Ph_3, generating the key transition-metal hydride complex CoH-H, which further reduces CO_2. Computational data reveal that the second pathway with an energy barrier of 18.3 kcal/mol is more favorable than the first one with an energy barrier of 27.2 kcal/mol.

For the conversion of CO_2 and CH_4, there are two different products, CH_3COOH and $HCOOCH_3$, following two different reaction routes. Both routes begin with the bonding of one CH_4 molecule to the metalloradical Co^0-C•Ph_3, and the bonding breaks one C-H bond with the H

bonded to the Co center. The subsequent hydride transfer has two possible pathways. One (pathway **PO**) is to the O atom of CO_2 and the other (pathway **PC**) is to the C atom of CO_2. By comparing with the rate-determining steps, we identified that the **PO** route with the energy barrier of 24.5 kcal/mol is more favorable for accomplishing the conversion of CO_2 and CH_4 into CH_3COOH than the PC route leading to $HCOOCH_3$.

This present Co^0-based metalloradical system represents a novel catalytic protocol that may contribute to the development of effectively utilizing small molecules (H_2 and CH_4) to reduce CO_2. We anticipate that this work can stimulate further theoretical and experimental studies on the catalytic applications of metal-stabilized radical system in the CO_2 reduction.

Conflicts of interest

There are no conflicts to declare.

Electronic supplementary information (ESI) available: The optimized structures of the metalloradical Co-C$^{\bullet}$Ph coordinated by a dipridy or a pentane-2,4-diimine and their geometric parameters; the transition state leading to the cobalt hydride complex CoH-H; partial molecular orbital energy levels of the metalloradical Co-C$^{\bullet}$Ph$_3$ (α orbital and its corresponding β orbital) and the atomic coordinates of intermediates and key transition states.

Acknowledgements

This work was supported by the National Natural Science Foundation of China (No. 21303065), Anhui University Natural Science Research Project (No. KJ2017A388), Approving and Initiating the Cultivation Project of Excellent Top-notch Talent in Colleges and Universities in Anhui Province (No.gxfx2017037). This work was performed in part at the Joint School of Nanoscience and Nanoengineering, a member of the Southeastern Nanotechnology Infrastructure Corridor (SENIC) and National Nanotechnology Coordinated Infrastructure (NNCI), which is supported by the National Science Foundation (Grant ECCS-1542174).

References

1. J. R. Bour, D. M. Ferguson, E. J. McClain, J. W. Kampf and M. S. Sanford, J. Am. Chem. Soc., 2019, **141**, 8914-8920.
2. X. Wen, Y. Wang and X. P. Zhang, Chem. Sci., 2018, **9**, 5082-5086.
3. H. Jiang, K. Lang, H. Lu, O. Wojtas and X. P. Zhang, J. Am. Chem. Soc, 2017, **139**, 9164-9167.
4. P. F. Kuijpers, Ir. J. I. vander Vlugt, S. Schneider and B. d. Bruin, Chem. Eur.J. , 2017, **23**, 13819-13829.
5. T.Büttner, J. Geier, G. Frison, J. Harmer, C. Calle, A. Schweiger, H. Schönberg, H. Grützmacher, Science. 2005, **307**, 235-238.
6. A. Gansäuer, S. Hildebrandt, E. Vogelsang and R. A. Flowers II, *Dalton Trans*, 2016, **45**, 448–452.
7. A. Gansäuer, S. Hildebrandt, A. Michelmann, T. Dahmen, D. von Laufenberg, C. Kube, G. D. Fianu and R. A. Flowers II, *Angew. Chem., Int. Ed.*, 2015, **54**, 7003–7006.
8. A. Studer and D. P. Curran, *Angew. Chem., Int. Ed. Engl*, 2016, **55**, 58–102.
9. H. Pellissier and H. Clavier, *Chem. Rev.*, 2014, **114**, 2775-2823.
10. H. Lu and X. P. Zhang, *Chem. Soc. Rev*, 2011, **40**, 1899–1909.
11. X. Xu, Y. Wang, X. Cui, L. Wojtas and X. P. Zhang, *Chem. Sci.,*, 2017, **8**, 4347.
12. Y. Wang, X. Wen, X. Cui, L. Wojtas and X. P. Zhang, *J. Am. Chem. Soc.*, 2018, **140**, 4792−4796.
13. Y. Hu, K. Lang, C. Li, J. B. Gill, I. Kim, H. Lu, K. B. Fields, M. K. Marshall, Q.-G. Cheng, X. Cui, L. Wojtas and X. P, Zhang, *J. Am. Chem. Soc*, 2019, **141**, 18160-18169.
14. K. Lang, S. Torker, L. Wojtas and X. P. Zhang, *J. Am. Chem. Soc.*, 2019, **141**, 12388–12396.
15. Y. W. Chan, B. de. Bruin, and K. S. Chan, *Organometallics*, 2015, **34**, 2849−2857.

16. D. Schluter, F. Kleemiss, M. Fugel, E. Lork, K. Sugimoto, S. Grabowsky, J. Harmer and M. Vogt, Chem. Eur.J., 2020, **26**, 1335-1343.
17. T. Schaub and R. A. Paciello, *Angew. Chem., Int. Ed.*, 2011, **50**, 7278−7282.
18. C. A. Huff and M. S. Sanford, *ACS Catal.*, 2013, **3**, 2412−2416.
19. S. Park, D. Bézier and M. Brookhart, *J. Am. Chem. Soc.*, 2012, **134**, 11404−11407.
20. A. Berkefeld, W. E. Piers, M. Parvez, L. Castro, L. Maron and O. Eisenstein, *Chem. Sci.,*, 2013, **4**, 2152−2162.
21. E. Balaraman, C. Gunanathan, J. Zhang, L. J. W. Shimon and D. Milstein, *Nature Chem.*, 2011, **3**, 609 −614.
22. A. Weilhard, M. I. Qadir, V. Sans and J. Dupont, *ACS Catal.*, 2016, **8**, 1628–1634.
23. S.Moret, P. J. Dyson and G. Laurenczy, *Nat. Commun.*, 2014, **5**, 4017.
24. TZ. Li, T. M. Rayder, L. Luo, J. A. Byers and C. Tsung, *J. Am. Chem. Soc*, 2018, **140**, 8082–8085.
25. A. Anaby, M. Feller, Y. Ben-David, G. Leitus, Y. Diskin-Posner, L. J. Shimon and D. Milstein, *J. Am. Chem. Soc.*, 2016,**138**, 9941–9950.
26. Q. Qian, J. Zhang, M. Cui and B. X. Han, *Nat. Commun.*, 2016, **7**, 11481.
27. C. Liu, J. Xie, G. Tian, W. Li and Q. L. Zhou, *Chem. Sci.,* 2015, **6**, 2928–2931.
28. R. Kanega, N. Onishi, D. J. Szalda, M. Z. Ertem, J. T. Muckerman, E. Fujita and Y. Himeda, *ACS Catal.*, 2017, **7**, 6426–6429.
29. T. Zhao, X. Hu, Y. Wu and Z. Zhang, *Angew. Chem. Int. Ed.*, 2019, **58**, 722–726.
30. S. N. Riduan, Y. Zhang and J. Y. Ying, *Angew. Chem.Int. Ed.*, 2009, **48**, 3322−3325.
31. G. Ung, G. D.Frey, W. W. Schoeller and G. Bertrand, *Angew. Chem. Int. Ed.*, 2011, **45**, 9923−9925.
32. G. Zeng, S. Maeda, T.Taketsugu and S. Sakaki, *J. Am. Chem. Soc*, 2016, **138**, 13481-13484.
33. W. Huang, K. C. Xie, J. P. Wang, Z. H. Gao, L. H. Yin and Q. M. Zhu *J. Catal.*, 2001, **201**, 100–104.

34. E. M. Wilcox, G. W. Roberts and J. J. Spivey, *Catalysis Today*, 2003, **88**, 83-89.

35. Y.H. Ding, W. Huang and Y.G. Wang, *Fuel Process. Technol.*, 2007, **88**, 319-324.

36. Y. Zhao, C. Cui, J. Han, H. Wang, X. Zhu and Q. Ge, *J. Am. Chem. Soc*, 2016, **138**, 10191–10198.

37. M. Gomberg, *J. Am. Soc. Chem.*, 1900, **22**, 757–771.

38. J. L. Kuo, J. Hartung, A.Han and J. R. Norton, *J. Am. Chem. Soc.*, 2015, **137**, 1036−1039.

39. G. Li, A. Han, M. E. Pulling, D. P. Estes and J. R. Norton, *J. Am. Chem. Soc.*, 2012, **134**, 14662−14665.

40. C. Sui-Seng, A. Hadzovic, A. J. Lough and R. H. Morris, *Dalton Trans.*, 2007, 2536−2541.

41. H. Guan, M. Limura, M. P. Magee, J. R. Norton and G. Zhu, *J. Am. Chem. Soc.*, 2005, **127**, 7805−7814.

42. S. Ghosh, G. Hogarth, N. Hollingsworth, K. B. Holt, S. E. Kabir and B. E. Sanchez, *Chem. Commun.* 2014, **50**, 945−947.

43. J. Y. Yang, S. E.Smith, T. Liu, W. G. Dougherty, W. A. Hoffert, W. S. Kassel, M. R. DuBois, D. L. DuBois and R. M. Bullock, *J. Am. Chem. Soc.*, 2013, **135**, 9700−9712.

44. M. J. Frisch, G. W. Trucks, H. B. Schlegel, G. E. Scuseria, M. A. Robb, J. R. Cheeseman, G. Scalmani, V. Barone, G. A. Petersson, H. Nakatsuji, X. Li, M. Caricato, A. V. Marenich, J. Bloino, B. G. Janesko, R. Gomperts, B. Mennucci, H. P. Hratchian, J. V. Ortiz, A. F. Izmaylov, J. L. Sonnenberg, D. Williams-Young, F. Ding, F. Lipparini, F. Egidi, J. Goings, B. Peng, A. Petrone, T. Henderson, D. Ranasinghe, V. G. Zakrzewski, J. Gao, N. Rega, G. Zheng, W. Liang, M. Hada, M. Ehara, K. Toyota, R. Fukuda, J. Hasegawa, M. Ishida, T. Nakajima, Y. Honda, O. Kitao, H. Nakai, T. Vreven, K. Throssell, J. A. Montgomery, Jr., J. E. Peralta, F. Ogliaro, M. J. Bearpark, J. J. Heyd, E. N. Brothers, K. N. Kudin, V. N. Staroverov, T. A. Keith, R. Kobayashi, J. Normand, K. Raghavachari, A. P. Rendell, J. C. Burant, S. S. Iyengar, J. Tomasi, M. Cossi, J. M. Millam, M. Klene, C. Adamo, R. Cammi, J. W. Ochterski, R. L. Martin, K. Morokuma,

O. Farkas, J. B. Foresman, and D. J. Fox,, *Gaussian 16; Gaussian, Inc.: Wallingford CT,* 2016.

45. A. D. Becke, *J. Chem. Phys.*, 1993, **98**, 5648−5652.
46. C. Lee, W. Yang and R. G. Parr, *Phys. Rev. B*, 1988, **137**, 785−789.
47. S.Grimme, J. Antony, S.Ehrlich, and H.Krieg, *J. Chem. Phys.*, 2010, **132**, 154104.
48. P. Singla, M. Riyaz, S. Singhal and N. Goel, *Phys. Chem. Chem. Phys.*, 2016, **18**, 5597--5604.
49. W. J. Hehre, R. Ditchfield and J. A. Pople, *J. Chem. Phys.*, 1972, **56**, 2257−2261.
50. K. Fukui, *Acc. Chem. Res.*, 1981, **14**, 363−368.
51. K. Fukui, *J. Phys. Chem.* , 1970, **74**, 4161−4163.
52. A. E. Reed, R. B. Weinstock and F. Weinhold, *J. Chem. Phys.*, 1985, **83**, 735.
53. J. E. Carpenter, C. M. Morales and F. Weinhold, *J. Mol. Struct.: THEOCHEM*, 1988, **169**, 41.
54. E. D. Glendenig, J. K. Badenhoop, A. E. Reed, J. E. Carpenter, J. A. Bohmann and C. M. Morales, F. Weinhold, *NBO 5.0, Theoretical Chemistry Institute, University of Wisconsin, Madison*, 2001.
55. A. E. Sherry and B. B. Wayland, *J. Am. Chem. Soc.*, 1990, **112**, 1259-1261.

Graphical Abstract

Two advantages of metalloradical: serve as an initiator of CO_2 reduction and provide transition metal hydrogen complex (TMHC).